Cardiovascular Research (2017) **113**, 633–643
doi:10.1093/cvr/cvx016

Osteopontin RNA aptamer can prevent and reverse pressure overload-induced heart failure

Jihe Li[1,2†], Keyvan Yousefi[2,3†], Wen Ding[2,3], Jayanti Singh[1,2], and Lina A. Shehadeh[1,2,4*]

[1]Department of Medicine, Division of Cardiology, University of Miami Leonard M. Miller School of Medicine, Miami, FL 33136, USA; [2]Interdisciplinary Stem Cell Institute, University of Miami Leonard M. Miller School of Medicine, Biomedical Research Building, Room 818, 1501 NW 10th Avenue, Miami, FL 33136, USA; [3]Department of Molecular and Cellular Pharmacology, University of Miami Leonard M. Miller School of Medicine, Miami, FL 33136, USA; and [4]Vascular Biology Institute, University of Miami Leonard M. Miller School of Medicine, Miami, FL 33136, USA

Received 29 June 2016; revised 21 September 2016; editorial decision 22 January 2017; accepted 24 January 2017; online publish-ahead-of-print 1 February 2017

Time for primary review: 39 days

Aims Cardiac myocyte hypertrophy, the main compensatory response to chronic stress in the heart often progresses to a state of decompensation that can lead to heart failure. Osteopontin (OPN) is an effector for extracellular signalling that induces myocyte growth and fibrosis. Although increased OPN activity has been observed in stressed myocytes and fibroblasts, the detailed and long term effects of blocking OPN signalling on the heart remain poorly defined. Targeting cardiac OPN protein by an RNA aptamer may be beneficial for tuning down OPN pathologic signalling. We aimed to demonstrate the therapeutic effects of an OPN RNA aptamer on cardiac dysfunction.

Methods and results *In vivo*, we show that in a mouse model of pressure overload, treating at the time of surgeries with an OPN aptamer prevented cardiomyocyte hypertrophy and cardiac fibrosis, blocked OPN downstream signalling (PI3K and Akt phosphorylation), reduced expression of extracellular matrix (Lum, Col3a1, Fn1) and hypertrophy (Nppa, Nppb) genes, and prevented cardiac dysfunction. Treating at two months post-surgeries with the OPN aptamer reversed cardiac dysfunction and fibrosis and myocyte hypertrophy. While genetic homozygous deletion of OPN reduced myocardial wall thickness, surprisingly cardiac function and myocardial fibrosis, specifically collagen deposition and myofibroblast infiltration, were worse compared with wild type mice at three months of pressure overload.

Conclusion Taken together, these data demonstrate that tuning down cardiac OPN signalling by an OPN RNA aptamer is a novel and effective approach for preventing cardiac hypertrophy and fibrosis, improving cardiac function, and reversing pressure overload-induced heart failure.

Keywords Cardiac hypertrophy • Cardiac fibrosis • Heart failure • Osteopontin • Aptamer • TAC

1. Introduction

Non-mitotic growth of cardiac myocytes is the major response of the heart to increased workload.[1] Whereas myocyte hypertrophy may be compensatory especially in its early stages, it becomes a major risk factor for heart failure when associated with comorbidities such as hypertension and myocardial infarction (MI). This is due at least in part to parallel changes in the expression of cytokines, extracellular matrix (ECM) proteins and increased interstitial fibrosis. Current therapy for pathologic hypertrophy is generally limited to targeting the down-regulation of associated signalling pathways by blocking the activities of upstream cell membrane receptors and ion channels.[2] Novel drug targets may be revealed through the identification of signalling cytokines that act through autocrine pathways. Osteopontin (OPN) is a pleiotropic extracellular signal-regulated bone sialoprotein whose activity is increased in myocytes[3–5] and fibroblasts[5,6] by most hypertrophic stimuli. Serum OPN levels are significantly increased in patients with heart failure and OPN constitutes an independent predictor of 4-year mortality in these patients.[4] Cardiac myocyte-specific over-expression of OPN in transgenic mice causes dilated cardiomyopathy and heart failure accompanied by myocarditis, T cell-mediated inflammation, and fibrosis.[7] Global knock

* Corresponding author. Tel: +1 305 243 0867; fax: +1 305 243 3906, E-mail: lshehadeh@med.miami.edu
† These two authors contributed equally.

down of OPN in mice reduces cardiac fibrosis after short term MI[8] or Angiotensin II infusions.[9,10]

Recently, small structured single-stranded nucleic acid ligands, also known as DNA or RNA aptamers, have emerged as alternatives to small molecule- and antibody-based therapies.[11,12] Aptamers, from the Latin word 'apto' meaning 'to fit', specifically bind target proteins with high affinity (high pico-molar to low nano-molar range), are stable, lack immunogenicity, and elicit biological responses. This high-affinity selective binding of aptamers can modulate 3D structures and thence properties of target proteins. Therefore, aptamers can be used for therapeutic purposes in much the same way as monoclonal antibodies.[13,14] However, aptamers have an additional advantage over monoclonal antibodies because their production involves relatively simple chemistry with no live organism involvement. Such cell-free technology offers significant advantages for developing and optimizing these molecules for translational therapeutics.

Unlike other nucleic acid-based therapies such as siRNA, DNA, and RNA, aptamers are unique because they generally do not directly affect steps preceding protein function such as transcription, splicing, RNA processing, or translation.[15] Another major advantage of aptamers is their ability to be conjugated with other oligonuclotides such as siRNAs[16–18] and miRNAs[19,20] for targeted delivery and enhanced therapeutic potency. Our objective in this study was to provide the first demonstration of an RNA ligand capable of blocking OPN pathologic cardiac signalling. Toward this end, we elected to use an aptamer against human OPN protein.[21] We characterized the effect of the OPN aptamer on prevention of heart failure at the cellular, molecular, and functional levels in mice subjected to transverse aortic constriction (TAC). Using wild type and *OPN*$^{-/-}$ mice subjected to TAC, we found impressive therapeutic effects by OPN aptamer treatment but not by OPN genetic homozygous deletion, in the treatment/reversal of heart failure. Taken together, these findings support a novel RNA platform for regulating OPN pathologic signalling in the hypertrophic heart.

2. Experimental procedures

Reagents: Antibody against GAPDH (sc-25778) was purchased from Santa Cruz Biotechnology (Santa Cruz, CA, USA); antibodies against FN1 (F3648) and SMA (A-5228) were obtained from Sigma–Aldrich (St. Louis, MO, USA); antibodies against PI3K (4249) and p-AKT (2965) were obtained from Cell Signalling (Danvers, MA, USA); antibodies against OPN (AF808), Lumican (AF2745), and OPN DuoSet ELISA kit (DY441) were purchased from R&D Systems (Minneapolis, MN, USA). Antibody against COLIII (600-401-105-0.1) was purchased from Rockland (Limerick, PA, USA). Amersham Femto Western detection system was obtained from GE Healthcare Bio-Sciences (Piscataway, NJ, USA). The MirVana PARIS kit used for RNA and protein isolations, reagents for real-time quantitative PCR, and Alexa Fluor-555 (W32464) and -488 (W11261) Wheat Germ Agglutinin (WGA) were obtained from Life Technologies (Carlsbad, CA, USA). Picrosirius Red Stain Kit was purchased from Polysciences (24901-250). The 40-nucleoetide OPN aptamer (5-mCrGrG mCmCrA mCrArG rArAmU rGrArA rArArA mCmCmU mCrAmU mCrGrA mUrGmU mUrGmC rAmUrA rGmUmU rG-3) and 35-nucleotide mutant OPN aptamer (5-mCrGrG mCmCrA mCrArG rArAmU rGrArA mUmCrA mUmCrG rAmUrG mUmUrG mCrAmU rArGmU mUrG-3) with 2'O-Methyl modification (m) at the Pyrimidines (Cytosines and Uracils) and un-modified (r) purines (Adenine and Guanine) were synthesized by IDT (Coralville, Iowa). The sequences were obtained from Mi *et al.*,[21] but the modifications (described above) are quite different from the ones used by Mi *et al.*[21] and Talbot *et al.*[22]

2.1 Animal work

All experiments involving animals were approved by the Institutional Animal Care and Use Committee at the University of Miami, conforming to NIH guidelines. Wild type (C57Bl6) and OPN knock-out mice (004936) were bought from Jackson Labs and bred in-house. While the OPN knock-out mice were originally characterized on 129xBlack Swiss hybrid background,[23,24] they were crossed for at least 10 generations with C57Bl6 mice before being donated to the Jackson lab. Therefore, the OPN knock-out mice used in this study are of more than 99% C57Bl6 background which is the same background used for the wild type mice in the aptamer study. For sacrificing all mice used in this study, isoflurane inhalation followed by cervical dislocation was used.

2.2 Transverse aortic constriction (TAC) and aptamer injections

Wild type C57BL6 or *OPN*$^{-/-}$ mice weighing 23–25 g were anesthetized with ketamine (130 mg/kg) and xylazine (10 mg/kg). Each mouse was placed supine on a heating pad to maintain body temperature at 37°C. An endotracheal intubation was rapidly performed and the cannula connected to a Mouse Ventilator (Model 845, Harvard Apparatus, MA, USA) with a stroke volume of 10 µl/g body weight of room air and respiratory rate of 120 breaths/min. Surgical procedures were performed using a stereo microscope (Omano OM2300S-GX4 Zoom Stereo Boom Microscope).The chest cavity was opened using two Dumont forceps to make a small incision at the level of the second intercostal space at the left upper sternal border. After the aortic arch was isolated, the transverse aorta was isolated between the carotid arteries and constricted by a 6-0 silk suture ligature tied firmly against a 27-gauge needle. The needle was promptly removed to produce an aortic constriction of 0.4 mm in diameter. The chest cavity was then closed with a 6-0 nylon suture. For prevention study, the left subclavian vein was exposed and 56 nmol/kg OPN aptamer, 56 nmol/kg mutant OPN aptamer or PBS—each in 0.1 mL volume was injected in left subclavian vein. This would constitute the first of 10 injections in the prevention study. The remaining nine injections were administered via tail vein as described below, once every other day starting at 2 days post-TAC. Anesthesia was maintained with ketamine and xylazine. The mouse was allowed to recover from anesthesia while its body temperature was maintained at 37 °C. Sham-operated animals underwent a similar surgical procedure without aortic constriction, to serve as controls. Transverse aortic flow velocities were obtained by pulsed wave (PW) Doppler using a 20° angle across the constriction site within 1 week post-surgery. The pressure gradient was estimated using the modified Bernoulli equation ($\Delta p = 4V^2$) and only mice with a pressure gradient >44 mmHg were used in the study, with the average pressure gradient = 62 mmHg (see Supplementary material online, *Tables SI and SII*).

For tail vein injections, the mouse was placed in a restrainer (Tail Veiner TV-150) and the tail was then warmed with a lamp. The tail was swabbed with 70% alcohol on a gauze sponge. The tail was held tightly with one hand and with the other hand, the needle was inserted parallel to the tail vein penetrating around 5 mm into the lumen while keeping the bevel of the needle facing upwards. The OPN aptamer, mutant OPN aptamer, or PBS solution was then injected slowly. When the intravenous administration was finished, the injection site was pressed firmly with

a swab to prevent backflow of the administered solution and/or blood. For the treatment study, a total of 14 tail vein injections were administered once every other day, starting at 2 months post-TAC.

2.3 Echocardiography

Cardiac function was evaluated by a Vevo 770 echocardiography imaging system (Visual Sonics) at baseline and 4, 8, and 12 weeks after sham or TAC surgery. Briefly, mice were anesthetized with 4% isoflurane at 0.8 L/min flow rate and maintained with 1% isoflurane. Following anesthesia, the mice were fixed in a supine position on a pad with an integrated temperature sensor, a heater, and ECG electrodes. The heart rate was monitored constantly and body temperature was maintained at 37 °C during measuring. Depilatory cream was used to remove fur from the region of interest, and medical ultrasonographic acoustic gel was used as a coupling fluid between the real-time microvisualization scan head and the skin. The B-mode 2 dimensional (2D) images and M-mode tracings of the anterior and posterior left ventricular (LV) wall were obtained using a 2D reference sector with a 707B scan head. Cardiac function parameters examined included LV B-Mode: Endocardial Area (d, diastole and s, systole); Endocardial Major (d,s); Endocardial Volume (d,s); Endocardial Stroke Volume; Endocardial % Ejection Fraction (EF); Endocardial Fractional Area Change (%FAC), FAC = (Endocardial Area;d - Endocardial Area;s)/(Endocardial Area;d); Endocardial Area Change; Endocardial Cardiac Output (CO). LV M-Mode: LVAW, Left ventricular anterior wall (d,s); LVID, Left ventricular internal diameter (d,s); LVPW, Left ventricular posterior wall (d,s); LV Vol, Left ventricle volume (d,s); %EF; % Fractional Shortening (FS), (FS = (LVID;d - LVID;s)/(LVID;d)); LV Mass; LV Mass Corrected, LV mass is corrected for mathematical overestimation (LV Mass Corrected = 0.8 (1.053((LVIDP;d + LVPW;d + IVS;d)^3 - LVID;D^3)), where 0.8 is the correction factor and 1.053 is the myocardial specific gravity). The data were analyzed with VEVO 770 software. Transverse aortic flow velocity was obtained by PW Doppler using a 20° angle across the constriction site within 1 week post-surgery. The pressure gradient was estimated using the modified Bernoulli equation ($\Delta p = 4V^2$) and only mice with a pressure gradient >44 mmHg were used in the study.

2.4 QPCR

RNA was extracted (Mirvana Paris kit) and gene transcripts were quantified by qPCR using Taqman assays for Nppa, Nppb, FN1, OPN, LUM, or COL3a1 on an ABI 7900HT thermocycler. For each group, fluorescence was plotted against the number of cycles on a logarithmic scale and data were normalized to the endogenous 18S control. The normalized cycle thresholds (delta Cts) were converted to fold change relative to the control group. For statistical analysis, ANOVA with Tukey post hoc correction was applied on the delta Cts.

2.5 Western blots

Protein concentration was measured using a Bradford assay. Samples were prepared and separated by a 4–12% Novex mini 15-well gradient gel (Bolt System, Life Technologies), and probed with OPN, FN1, PI3K, p-AKT or GAPDH antibody. Signals were detected by chemiluminescence (Femto, Thomas Scientific) on photographic films. Digitized images were analyzed using Image J (NIH). Protein band densitometry was normalized to that of GAPDH, and the averaged results were plotted as normalized densitometry units (n.d.u.). For statistical analysis, ANOVA with Tukey post hoc correction was applied on n.d.u.

2.6 Histochemistry

Dissected left ventricles or full hearts were weighed and then fixed in 10% formalin and embedded in paraffin. De-paraffinized 4 μm LV cross sections were stained with Picrosirius Red Stain Kit or Alexa Fluor 555- or -488 WGA as recommended by the manufacturers. Myocyte area was measured in Image J from WGA images captured on a Zeiss fluorescence microscope. At least five 32× objective fields per heart were used. Collagen content was assayed using the Picrosirius Red stained sections and polarized light microscopy for at least three 5× objective fields per heart. For SMA analyses, six images per cross section were captured at 10× magnification on a Zeiss fluorescence microscope, and the positive non-vascular area was quantified in Image J. For statistical analysis, ANOVA with Tukey post hoc correction was applied on the averages of myocyte area, % collagen per cross section, or % interstitial SMA per cross section. For H&E and WGA staining of four-chamber slices of the hearts, de-paraffinized 4 μm sagittal sections were used. The WGA imaging of sagittal sections was performed with a 10× objective on a Zeiss confocal using 10 z-stacks and tiling tools to cover the entire sections.

2.7 Statistics

For all experiments, *N* refers to the number of individual mice. All data are expressed as mean ± s.e.m. All *p*-values were calculated using ANOVA and corrected for multiple comparisons using Tukey post hoc correction. For the time series echo data in *Figure 5* and *Table IV* in Supplementary material online, Repeated Measures ANOVA with Tukey post hoc correction was applied when following the same mice over time. For survival curve, Kaplan–Meier with Log Rank test was performed. Repeated symbols represent *p*-values of different orders of magnitude, i.e. $^*P \leq 0.05$, $^{**}P \leq 0.01$.

3. Results

3.1 OPN progressively increases in the heart after pressure overload

To validate increased OPN expression in cardiac hypertrophy, we downloaded a publicly available microarray dataset on mouse hearts subjected to TAC for 2, 10, or 21 days (GSE1621). In that experiment by Zhao *et al.*, global gene expression profiling was performed on hearts from 3-month-old FVB male mice subjected to cardiac pressure overload by TAC.[25] Hearts were examined 2, 10, and 21 days after surgery.[25] We found a progressive increase in gene expression of OPN and other ECM molecules (FN1, LUM, COL3a) and the expected heart failure markers (Nppa and Nppb) as shown in Supplementary material online, *Figure SI*. These results validate the use of the mouse TAC model for targeting OPN signalling.

3.2 OPN aptamer substantially prevented cardiac dysfunction after pressure overload

To explore whether blocking OPN signalling by an OPN RNA Aptamer can prevent the heart from hypertrophy and dysfunction, we conducted TAC or sham surgeries using adult male C57BL6 mice. To synchronize the aortic constriction with OPN aptamer cardiac dysfunction prevention effect, we performed left subclavian vein injection with 56 nmole/kg of OPN Aptamer (Apt), 56 nmole/kg mutant OPN aptamer (M-Apt) or PBS as soon as the aortic arch was constricted. Then a total of nine tail vein injections were administered, one every 2 days. Cardiac function was measured by echocardiography at 4, 8, and 12 weeks post-TAC (*Figure 1A*). At 4 weeks post-TAC, the OPN aptamer group showed 25%

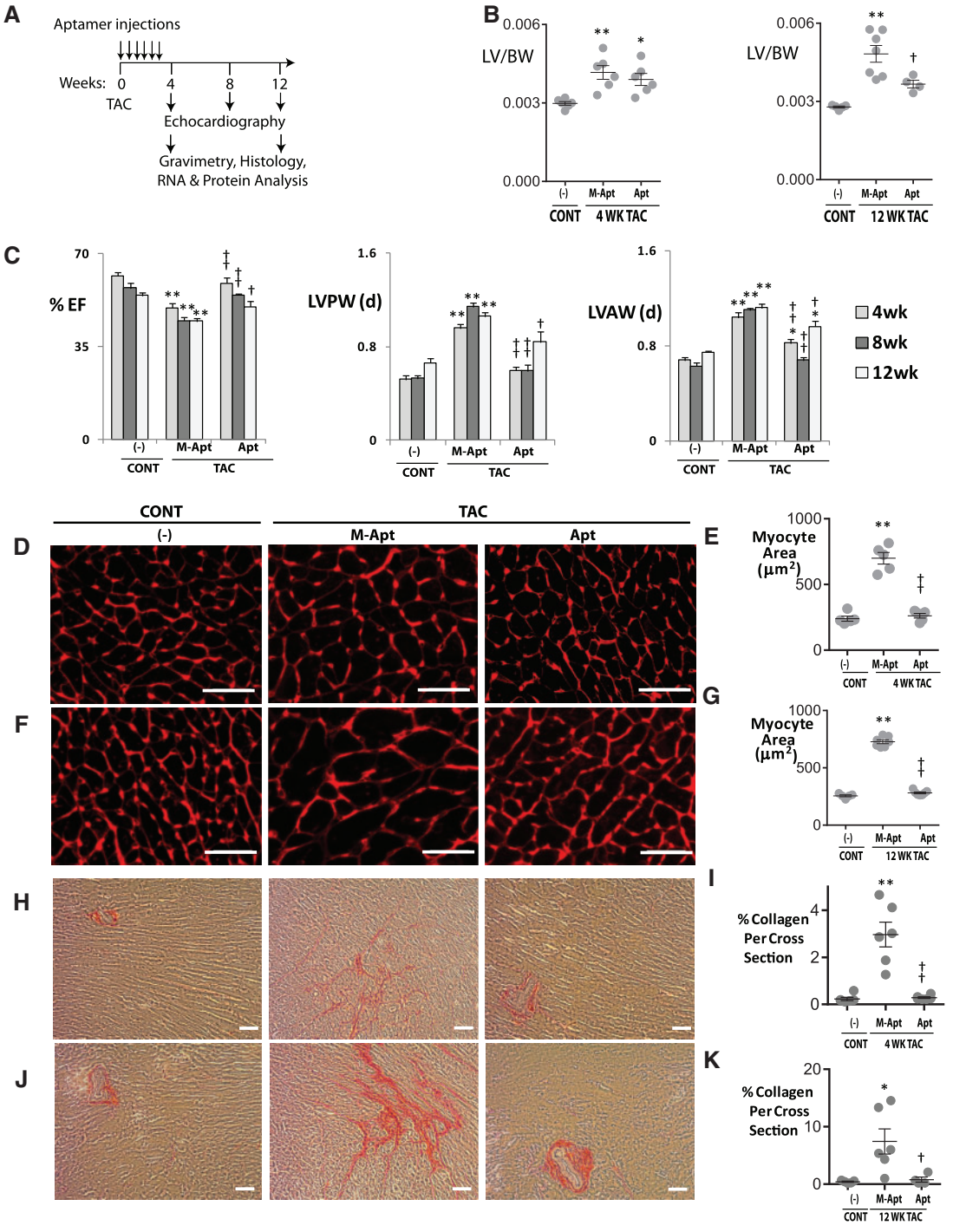

Figure 1 OPN aptamer prevents cardiac dysfunction, hypertrophy, and fibrosis in TAC mice. (*A*) Protocol for OPN aptamer therapy in the mouse TAC heart failure model. A total of 10 injections were administered, one subclavian and nine tail vein injections. (*B*) Effect of OPN aptamer on LV to body weight ratios, and (*C*) echocardiographic indices. Representative images of Wheat Germ Agglutinin staining and corresponding myocyte area of LV cross sections at 4 (*D*,*E*) and 12 weeks (*F*,*G*) post-TAC after systemic injections of OPN aptamer (Apt) or mutant OPN aptamer (M-Apt). Representative images of Picrosirius Red staining and corresponding % collagen quantification of LV cross sections at 4 (*H*,*I*) and 12 weeks (*J*,*K*) post-TAC after systemic injections of OPN aptamer or mutant OPN aptamer. Detailed echocardiographic data and statistics are shown in Supplementary material online, *Table SI*. Error bars represent SEM. *P*-values are from ANOVA with Tukey multiple correction. $^{*}P \leq 0.05$ vs. Sham; $^{**}P \leq 0.01$ vs. Sham; $^{\dagger}P \leq 0.05$ vs. TAC + M-Apt; $^{\dagger\dagger}P \leq 0.01$ vs. TAC + M-Apt. *n*, 5–13 mice per group. Cont, sham or no-surgery controls; TAC, Transverse Aortic Constriction; EF, Ejection Fraction; LVPW, LV posterior wall; LVAW, LV anterior wall; Scale bar, 50 μm.

improvement in Endocardial percent ejection fraction (%EF), 31% increase in Endocardial percent fractional area change (%FAC), 37% decrease in diastolic left ventricular posterior wall (LVPWd) thickness, and 31% decrease in Left Ventricular Mass Corrected—$P < 0.01$ for all, relative to mutant control group ($n = 13$ per group). Similar significant improvement was observed relative to the PBS group ($n = 3$) with no significant difference between the Sham and no-surgery groups ($n = 11$). This significant cardiac improvement was sustained at 8 weeks ($n = 7$ per group) and 12 weeks ($n = 4$–7 per group) post-surgery (*Figure 1C*, see Supplementary material online, *Figure SII*, and *Table SI*).

3.3 OPN aptamer effectively prevented LV remodelling after pressure overload

To investigate whether blocking OPN signalling via OPN aptamer can prevent cardiac myocyte hypertrophy and fibrosis, we conducted histological studies on 4 and 12 weeks paraffin embedded LV sections. WGA staining showed that the OPN aptamer treatment significantly reduced myocyte cross sectional area by 20% at 4 weeks and 30% at 12 weeks post-TAC—$P < 0.01$ for all (*Figure 1D–G*). Picrosirius Red staining showed that OPN aptamer reduced total cardiac fibrosis by 60% ($P < 0.01$) at 4 weeks, and 70% ($P < 0.05$) at 12 weeks post-TAC (*Figure 1H–K*). For each mouse section, six images were acquired and analyzed and 4–7 mice per group were used.

To examine the effect of blocking OPN signalling via OPN aptamer on LV weight after pressure overload, we weighed the dissected left ventricles, and normalized to body weight. We found that at 12 weeks post-TAC, OPN aptamer normalized LV weight by 24% ($P = 0.03$) relative to the mutant aptamer group ($n = 5$–7 per group; *Figure 1B*).

3.4 OPN aptamer reduces expression of ECM and heart failure genes and proteins

To study the effect of blocking OPN signalling via OPN aptamer on the expression of ECM and heart failure genes and proteins, we performed qPCR, western blot and Elisa on LV and right ventricular (RV) samples at 4 and 12 weeks post-TAC. The qPCR results showed that at 4 and/or 12 weeks post-TAC, OPN aptamer treatment significantly reduced the transcript expression of the LV heart failure markers Nppb (Natriuretic Peptide B), ECM proteins OPN, FN1 (Fibronectin 1), Col IIIa1 (collagen type IIIa1), and Lum (Lumican) relative to the mutant aptamer group ($n = 3$–6/group—*Figure 2A*). In the 4 week LVs, western blot quantification showed that OPN and downstream targets FN1, PI3K (110α) protein expression, as well as phosphorylation of Akt (p-Akt-Thr308) were significantly reduced in the OPN aptamer-treated samples relative to mut group ($n = 4$–5/group—*Figure 2B*). OPN protein down-regulation in the 4 week LVs was also confirmed by sandwich ELISA ($n = 5$/group—*Figure 2C*). To investigate whether the observed changes in gene and

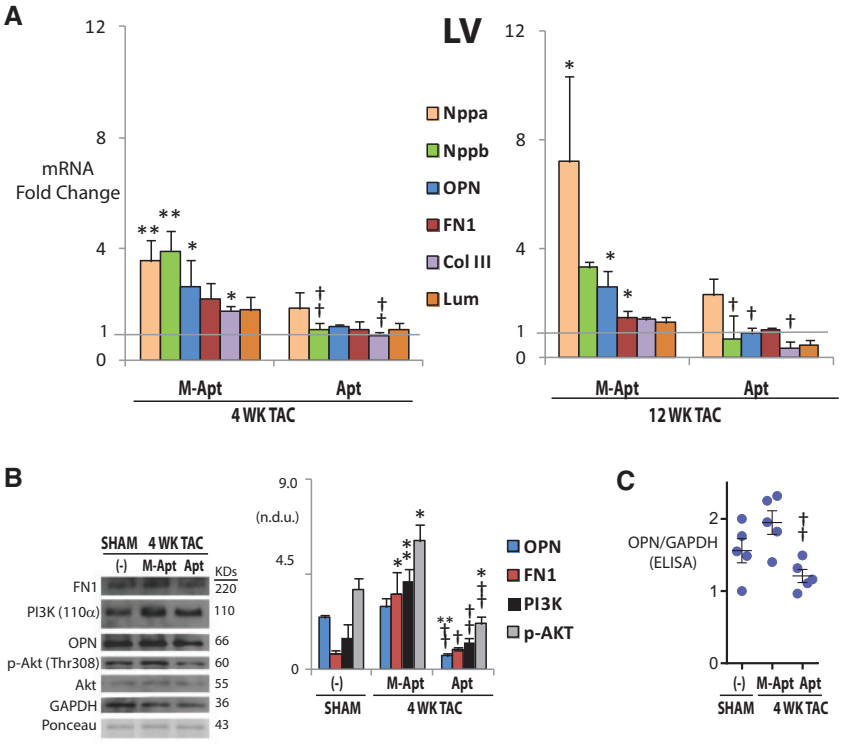

Figure 2 OPN aptamer reduces gene expression of extracellular matrix and heart failure genes and inhibits OPN signalling pathway in left ventricles (LVs). (*A*) Changes of mRNA expression as measured by qPCR at 4 and 12 weeks post-TAC after systemic injections of OPN aptamer (Apt) or mutant OPN aptamer (M-Apt). (*B* and *C*) Changes of protein expression as measured by western blot and corresponding quantification, or Elisa—at 4 weeks post-TAC after systemic injections of OPN aptamer or mutant OPN aptamer. Error bars = SEM. *P*-values are from ANOVA with Tukey multiple correction. *$P \leq 0.05$ vs. Sham; **$P \leq 0.01$ vs. Sham; †$P \leq 0.05$ vs. TAC + M-Apt; ††$P \leq 0.01$ vs. TAC + M-Apt. $n = 5$–7 mice per group. Nppa, Natriuretic Peptide A; Nppb, Natriuretic Peptide B; OPN, Osteopontin; FN1, Fibronectin 1, Col III, pro-alpha1 (III) collagen; Lum, Lumican; n.d.u.= normalized densitometry units; TAC, Transverse Aortic Constriction.

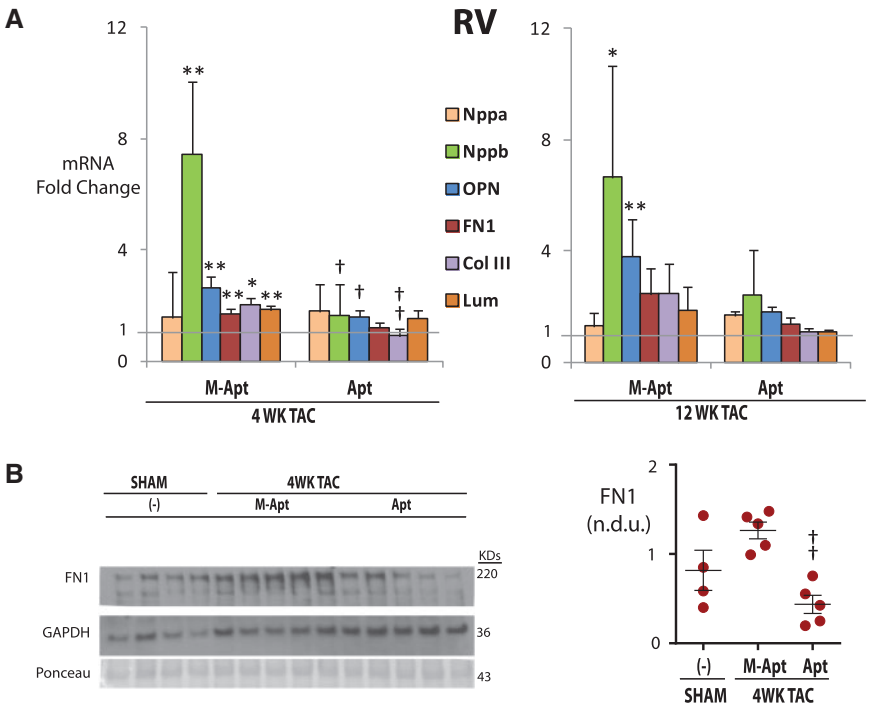

Figure 3 OPN aptamer reduces gene expression of extracellular matrix and heart failure genes in right ventricles (RVs). (*A*) Changes of mRNA expression as measured by qPCR at 4 and 12 weeks post-TAC after systemic injections of OPN aptamer (Apt) or mutant OPN aptamer (M-Apt). (*B*) Changes of FN1 protein expression as measured by western blot and corresponding quantification, at 4 weeks post-TAC after systemic injections of OPN aptamer or mutant OPN aptamer. Error bars = SEM. p-values are from ANOVA with Tukey multiple correction. $^{*}P \leq 0.05$ vs. Sham; $^{**}P \leq 0.01$ vs. Sham; $^{\dagger}P \leq 0.05$ vs. TAC + M-Apt; $^{\dagger\dagger}P \leq 0.01$ vs. TAC + M-Apt. $n = 4$–7 mice per group. Nppa, Natriuretic Peptide A; Nppb, Natriuretic Peptide B; OPN, Osteopontin; FN1, Fibronectin 1, Col III, pro-alpha1 (III) collagen; Lum, Lumican; n.d.u., normalized densitometry units; TAC, Transverse Aortic Constriction.

protein expression were unique to the LVs, we similarly quantified the expression of these genes and/or proteins in the RVs and atria. We found a similar pattern of expression in the RVs in the corresponding groups at 4 week post-TAC. Gene expression of Nppb, OPN and Col III was reduced at 4 weeks post-TAC in the RVs relative to mutant aptamer group ($n = 3$–7/group—*Figure 3*) but not at 12 weeks and nor in the atria (data not shown). The FN1 protein was significantly reduced in the RVs at 4 weeks post-TAC under the OPN Apt treatment ($n = 3$/group—*Figure 3B*). Since the OPN aptamer works by directly binding to the OPN protein and blocking its signalling,[21] these results indicate that blocking OPN signalling by the OPN aptamer can subsequently prevent cardiac dysfunction by blocking the hypertrophic, fibrotic, and gene expression programs that are otherwise activated during ventricular remodelling in pressure overload.

3.5 OPN aptamer reverses heart failure in wild type but not *OPN*$^{-/-}$ mice

To investigate the effect of OPN aptamer on reversal of cardiac remodelling rather than prevention and confirm that indeed the aptamer functions via OPN protein rather than non-specific binding, wild type and *OPN*$^{-/-}$ mice were subjected to Sham or TAC surgeries for 2 months after which systemic injections of OPN aptamer or mutant aptamer were administered every other 1 or 2 days until a total of 14 injections was reached (Outline shown in *Figure 4D*). At 2 months (before injections) and 2.5 months (after injections) post-TAC, cardiac function was assessed by echocardiography, and at 3 months histology on sagittal cardiac tissue was performed. OPN aptamer significantly reversed pathological remodelling of the wild type but not the *OPN*$^{-/-}$ hearts (*Figure 4B* and *C*). In fact, the highest mortality (~50%) was in all the *OPN*$^{-/-}$ mice post 2 month of TAC (Kaplan–Meier analysis, see Supplementary material online, *Figure SIII*). These banded *OPN*$^{-/-}$ mice had significantly higher normalized heart and lung weights (Supplementary material online, *Figure SIV*) suggesting congestive heart failure. The OPN aptamer rescue data in the wild type mice demonstrates that OPN aptamer is working through OPN protein and that the OPN signalling pathway can be interrupted in the late pathologic stages of cardiac hypertrophy to yield therapeutic benefits. Interestingly, the results suggest that the aptamer approach is superior to genetic homozygous deletion perhaps by permitting a certain amount of compensatory response without totally eliminating ability of ventricle to respond.

Figure 4B shows the echocardiographic M-mode images of the *same* mice at 2 months (before treatment) and then 2.5 months (after treatment) of TAC and corresponding echocardiographic time series data (*Figure 5*), is a compelling evidence on how the OPN aptamer can reverse LV remodelling. Detailed echocardiographic data at 3 month post-Sham/TAC, gravimetry data at 3 month post-Sham/TAC, and echocardiographic data at 1, 2, and 2.5–3 months post-TAC are shown in Supplementary material online, *Tables SII–SIV*, respectively.

To investigate whether blocking OPN signalling via OPN aptamer or genetic homozygous deletion can affect cardiac myocyte hypertrophy and fibrosis, we conducted histological studies on 3 month post-TAC paraffin embedded wild type and *OPN*$^{-/-}$ heart cross sections. WGA

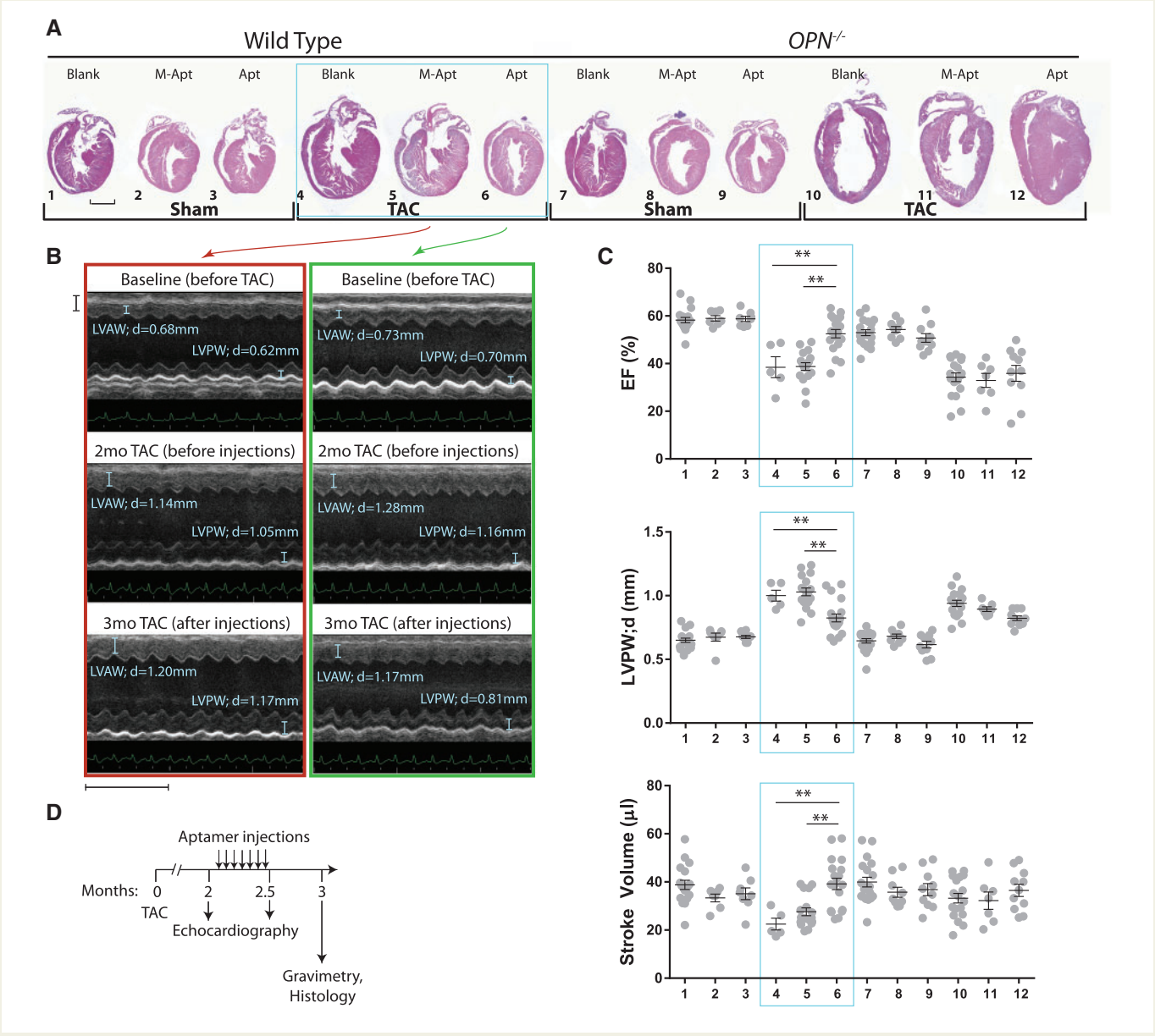

Figure 4 OPN aptamer reverses cardiac dysfunction in TAC wild type but not *OPN*$^{-/-}$ mice. (*A*) H&E sagittal heart sections of WT and *OPN*$^{-/-}$ mice subjected to Sham or TAC surgeries showing that OPN aptamer treatment significantly reversed pathological remodelling of the WT (but not the *OPN*$^{-/-}$) TAC hearts. Scale bar = 2 mm. (*B*) Representative images of M-mode echocardiography at papillary muscle level before and after injections show the reversal of cardiac hypertrophy in aptamer-injected TAC hearts. Images within the red or green panel belong to the same M-apt- or Apt-injected TAC mouse, respectively. Horizontal Scale bar = 1 mm and Vertical Scale bar = 5 mm. (*C*) Cardiac function is significantly improved in Aptamer-treated WT TAC mice. Horizontal lines in the graphs represent means. (*D*) Protocol for OPN aptamer therapy in the mouse TAC heart failure model. A total of 14 tail vein injections were administered. Error bars = SEM. *P*-values are from ANOVA with Tukey multiple correction. **P* ≤0.05. ***P* ≤0.01. N = 5–19 mice per group. WT, wild type; TAC, Transverse Aortic Constriction; M-Apt, mutant aptamer; Apt, OPN aptamer; EF, Ejection Fraction; LVPWd, Left Ventricular Posterior Wall, diastole. Detailed echocardiographic data and statistics are shown in Supplementary material online, *Table SII*.

staining showed that the OPN aptamer treatment significantly reduced myocyte hypertrophy in the 3 month TAC hearts relative to the mutant-aptamer-treated 3 month TAC hearts (*Figure 6A*). Interestingly, the *OPN*$^{-/-}$ TAC hearts did not show any myocyte hypertrophy (*Figure 6A*). For fibrosis, Picrosirius Red quantification showed significant reduction of fibrosis by the OPN aptamer in the wild type TAC hearts (*Figure 6B*). Surprisingly, the *OPN*$^{-/-}$ TAC hearts were extremely fibrotic/collagen-rich (*Figure 6B*). To identify the source of collagen deposition, we stained for the myofibroblast marker Smooth Muscle Actin (SMA). We found that the *OPN*$^{-/-}$ TAC hearts had excessive myofibroblasts infiltration (*Figure 7A* and *B*). To further confirm the increased myocardial fibrosis in the *OPN*$^{-/-}$ TAC hearts relative to the wild type TAC hearts, we performed WGA staining on heart sagittal sections and imaged using confocal z-stack and tiling tools. Previous studies have shown that WGA could also be used to quantify myocardial fibrosis with almost perfect correlation and improved visibility to Picrosirius Red.[26] Confirming our

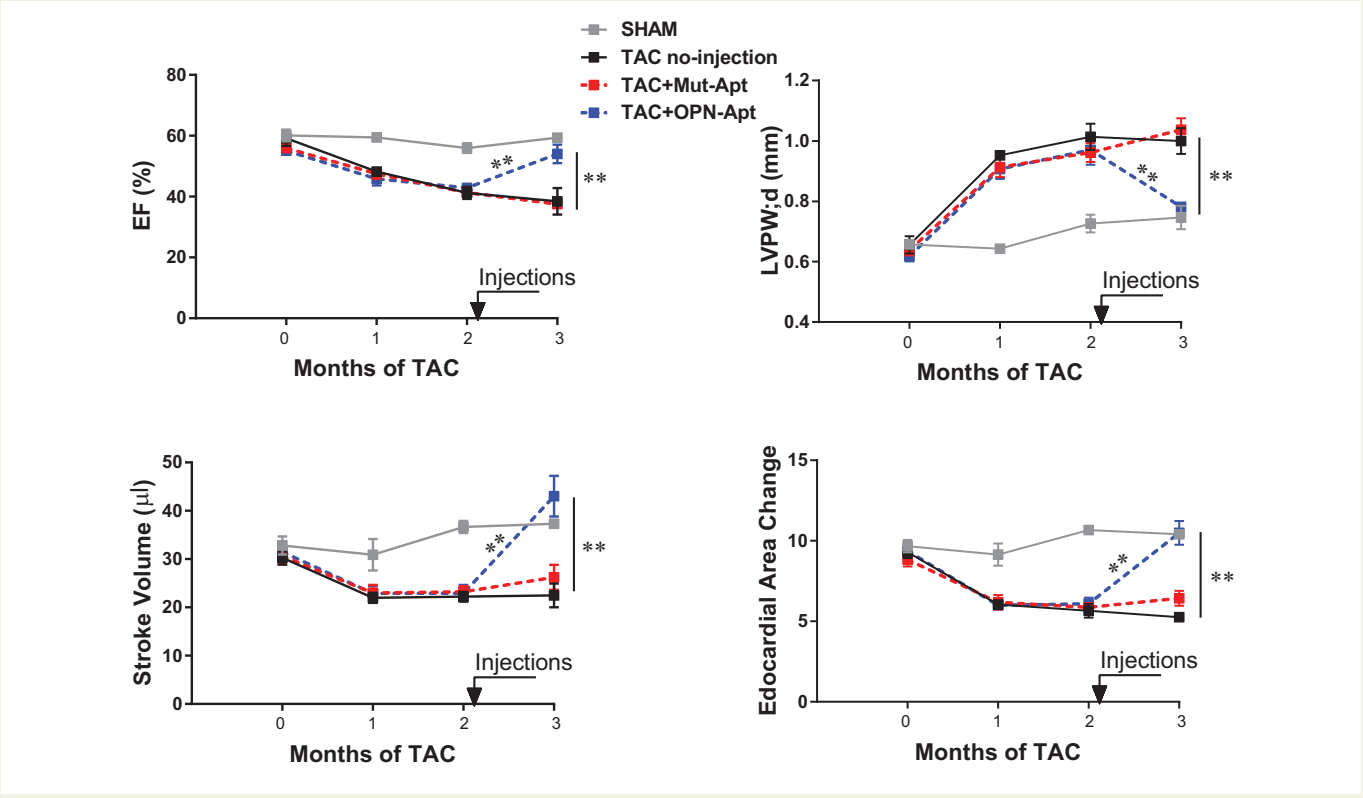

Figure 5 OPN aptamer reverses cardiac dysfunction in TAC wild type mice. Echocardiographic time series at baseline or 1 month-, 2 month (before injections)-, and 2.5 month (after injections)-post-TAC show significant improvement in cardiac function of OPN aptamer-injected mice. Detailed echocardiographic data and statistics are shown in Supplementary material online, *Table SIV*. $N = 3$-6 mice per group. Error bars = SEM. *P*-values are from Repeated Measures ANOVA with Tukey post hoc correction when following the same mice over time. $^{**}P \leq 0.01$. WT, wild type; TAC, Transverse Aortic Constriction; OPN-Apt, OPN aptamer; Mut-Apt, Mutant aptamer; EF, Ejection Fraction; LVPWd, Left Ventricular Posterior Wall, diastole.

Picrosirius Red fibrosis data, the WGA staining showed excessive fibrosis in the *OPN*$^{-/-}$ 3-month TAC hearts relative to the wild type 3-month TAC hearts (*Figure 7C*). For each mouse section, 4–6 images were acquired and analyzed and 4–7 mice per group were used. These data suggest that the fibrosis phenotype shown by myofibroblast infiltration and collagen deposition in the *OPN*$^{-/-}$ TAC hearts is responsible for their dysfunction.

4. Discussion

Here, we present the first report on the use of an RNA aptamer to prevent and treat heart failure in an experimental model. We report that a 40-nucleotide OPN aptamer[21] can prevent cardiac dysfunction in a pressure overload mouse model of cardiac hypertrophy. The injection of TAC mice with an OPN aptamer starting at the onset of TAC reduced myocyte hypertrophy and cardiac fibrosis in early (4 week) and late (12 week) TAC. The cardioprotection conferred by the OPN aptamer was associated with decreased heart failure-, fibrosis-, and ECM gene and/or protein expression in the left and right ventricles of the treated mice. Furthermore, the OPN aptamer injections prevented downstream signalling pathway of OPN that include expression of PI3K and phosphorylation of Akt.[10] Since the OPN aptamer works by directly binding to the OPN protein and blocking its signalling,[21] our results indicate that blocking OPN signalling by the OPN aptamer can subsequently prevent cardiac dysfunction by blocking the hypertrophic, fibrotic, and gene expression programs that are otherwise activated during ventricular remodelling in pressure overload. The dynamic changes in the levels of OPN and activated ECM proteins apparent at 4 weeks of TAC begin to plateau after 12 weeks suggesting that interventions in OPN signalling must be implemented before the 12 week time point in this model (see Supplementary material online, *Figure SV*). The beneficial effects of reducing OPN signalling along with the associated myocardial hypertrophy and fibrosis in the early phase of hypertrophy highlight the importance of the remodelling/adaptive phase in driving the pathological phase.

Impressively, systemic OPN aptamer treatment of two month-TAC mice succeeded in reversing heart failure in wild type but not *OPN*$^{-/-}$ mice. Surprisingly, while genetic homozygous deletion of OPN reduced LV wall thickness in late TAC mice, it caused deteriorated cardiac function compared with wild type mice and increased myocardial fibrosis. Echocardiographic time series data showed impressive rescue of cardiac function in the OPN-aptamer treated group. These data suggest that cardio-protection is not conferred by total deletion of OPN but rather by selectively tuning down the pathological aspect of OPN signalling as it is activated during cardiac hypertrophy and heart failure. Our findings indicate that the aptamer approach is superior to genetic homozygous deletion perhaps because aptamers intercede at the level of pathological hypertrophy while retaining levels of compensatory and/or other OPN-regulated immunological processes that are beneficial.[27] Alternatively, the total absence of OPN from birth onwards in the OPN knockout

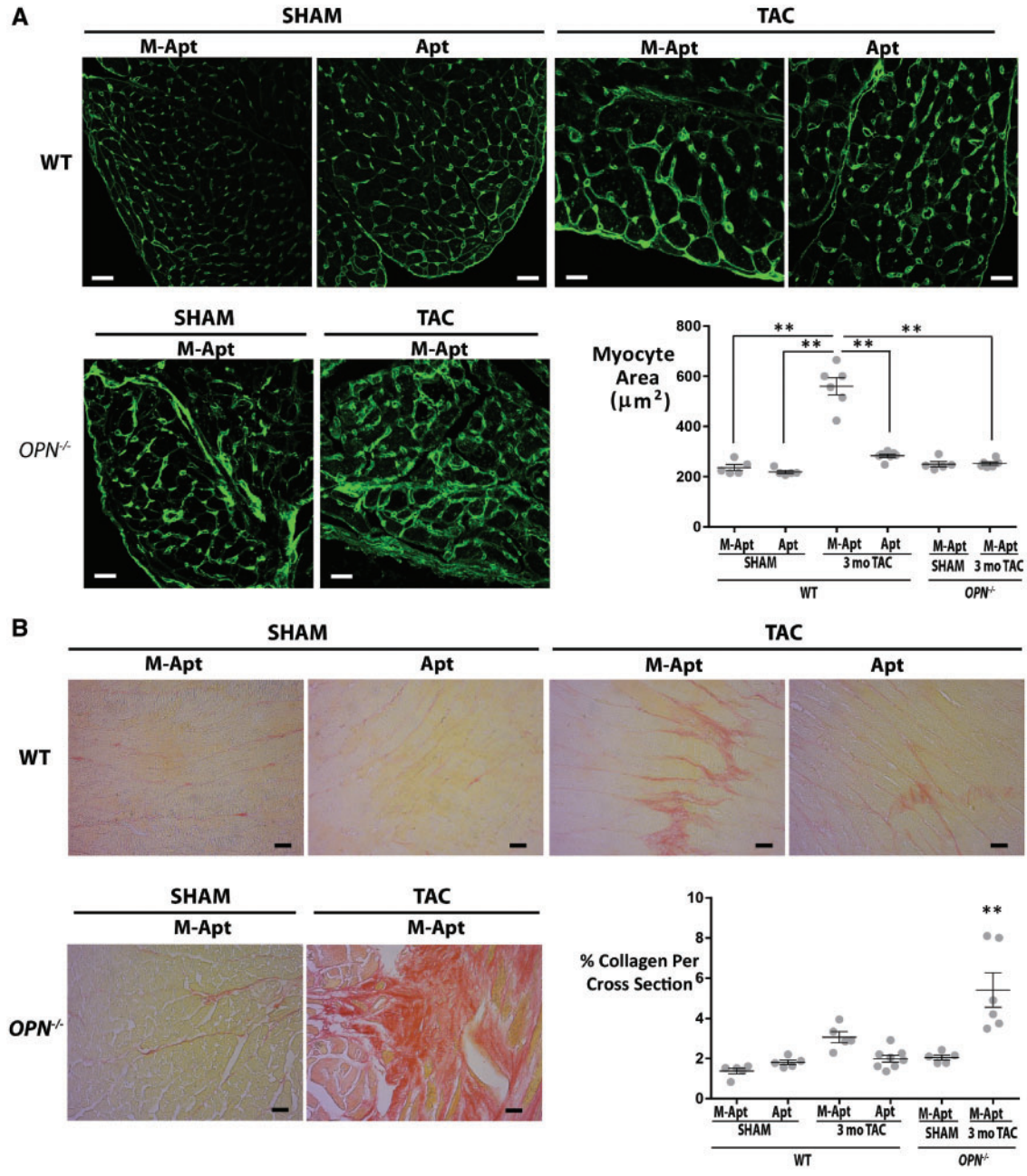

Figure 6 OPN aptamer reverses myocyte hypertrophy and fibrosis in wild type TAC hearts, and *OPN*$^{-/-}$ late TAC hearts show excessive fibrosis. (*A*) Representative images of Wheat Germ Agglutinin staining and corresponding myocyte area in heart cross sections at 3 month post-Sham ($N = 5$ mice per group) or TAC ($N = 6$–7 mice per group) in wild type and *OPN*$^{-/-}$ mice. Scale bar = 20μm. $^{**}P \leq 0.01$. (*B*) Representative images of Picrosirius Red staining and corresponding % collagen content in heart cross sections at 3 month post-Sham ($N = 5$ mice per group) or TAC ($N = 5$–8 mice per group) in wild type and *OPN*$^{-/-}$ mice. Scale bar = 20 μm. $^{**}P \leq 0.01$ relative to each of the other five groups. Error bars = SEM. *P*-values are from ANOVA with Tukey multiple correction. WT, wild type; TAC, Transverse Aortic Constriction; Apt, OPN aptamer; M-Apt, Mutant aptamer.

mice may elicit initially benign compensatory responses that drive the heart into failure once subjected to pathological overload. Either way, aptamers represent a highly translational approach for pathological hypertrophy. Our findings are in line with a recent report showing that inhibition of OPN by shRNA injected directly into the myocardium of a mutant Troponin mouse model of dilated cardiomyopathy could reduce LV remodelling and dysfunction.[28]

We found that *OPN*$^{-/-}$ hearts develop excessive fibrosis which is likely the cause for the more deteriorated cardiac function at 3 month TAC compared with wild type hearts. The finding that OPN deficiency causes increased collagen deposition after TAC was previously observed by Xei *et al.*[24] who reported a similar trend of increased collagen in *OPN*$^{-/-}$ versus wild type hearts at 1 month TAC. However, contradictory findings on fibrosis were reported when different stressors, Angiotensin II and

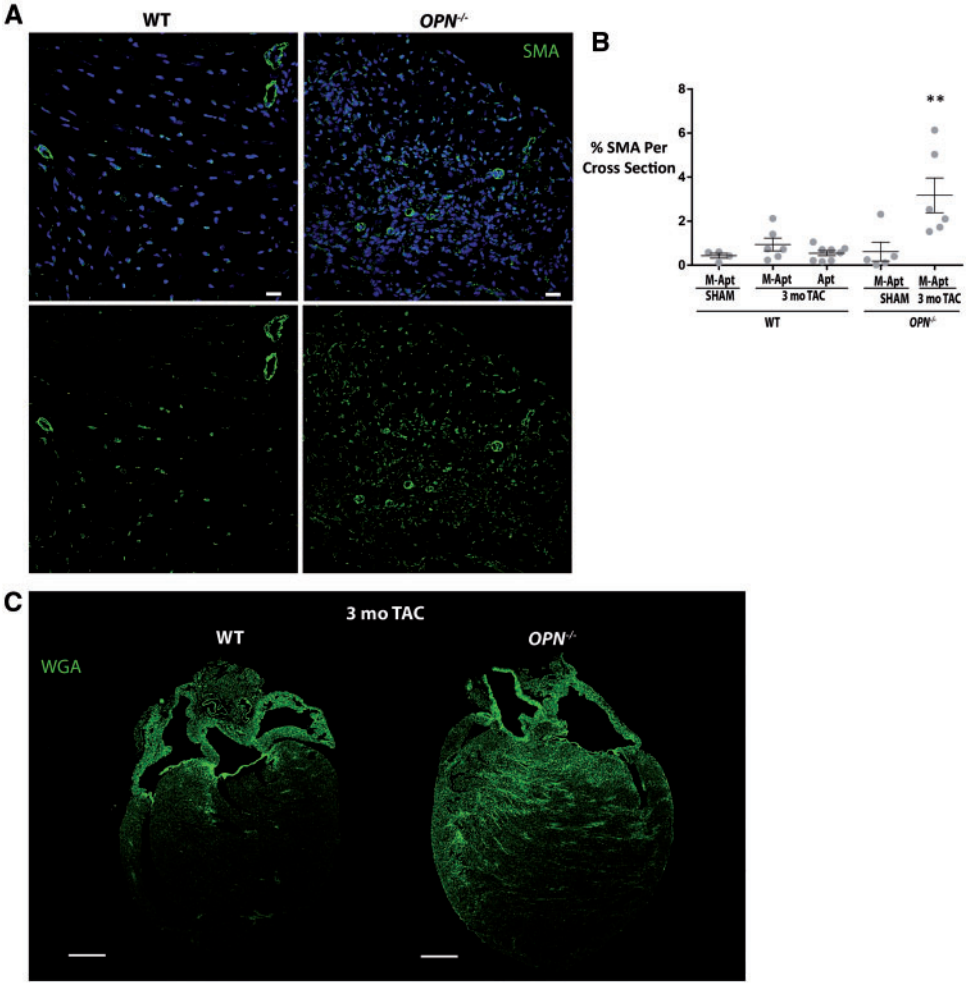

Figure 7 At late TAC, *OPN*$^{-/-}$ hearts have more fibrosis that wild type hearts. (*A*) Representative confocal images of SMA immonostaining in 3 month TAC WT and *OPN*$^{-/-}$ hearts showing excessive myofibroblast infiltration in the *OPN*$^{-/-}$ TAC hearts. (*B*) Quantification of interstitial SMA immunostaining in heart cross sections at 3 month post-Sham ($N = 4$–5 mice per group) or TAC ($N = 6$–8 mice per group) in WT and *OPN*$^{-/-}$ mice. Scale bar = 20 μm. Error bars = SEM. *P*-values are from ANOVA with Tukey multiple correction. $^{**}P \leq 0.01$ relative to each of the other four groups. (*C*) Representative confocal images of Wheat Germ Agglutinin staining in heart sagittal sections at 3 month post-TAC in WT and *OPN*$^{-/-}$ mice, showing excessive fibrosis in the *OPN*$^{-/-}$ hearts. Scale bar = 1 mm. WT, wild type; TAC, Transverse Aortic Constriction; Apt, OPN aptamer; M-Apt, Mutant aptamer.

MI, were used in OPN deficient mice in which myocardial fibrosis was less than in wild type mice.[8–10] We also found that *OPN*$^{-/-}$ mice at 3 month post-TAC did not display myocyte hypertrophy at the cellular level (in spite of a trend for increased LVPW thickness). This is in conflict with the results of Xie *et al.*[24] who reported significantly increased myocyte cross-sectional area in *OPN*$^{-/-}$ TAC hearts. The discrepancy concerning myocyte area could be due to the fact that the *OPN*$^{-/-}$ mice in our study were of C57Bl6 background while the ones used by Xie *et al.* were of 129/Black Swiss hybrid background (as explained in *Animal work*). In addition, Xie *et al.* reported myocyte area at 1-month post-TAC and may have missed the effects of OPN deletion at later stages. However, the reported increase in myocyte size by Xie *et al.* was significantly lower than that of WT animals after TAC.[24] Consistent with our results but with a different stressor from TAC, Trueblood *et al.* also reported an absence of myocyte hypertrophy in *OPN*$^{-/-}$ compared with wild type myocytes at 1 month post-MI.[8]

While cardiac hypertrophy and fibrosis usually happen in parallel during cardiac remodelling, the two pathologies may be mutually exclusive in certain cases. For example, Angiotensin II-induced cardiac remodelling in tissue inhibitor of metalloproteinase (TIMP) knockout mice was shown to cause distinct cardiac phenotypes depending on the TIMP type deficiency.[29] Specifically, with Ang II infusions, *TIMP2*$^{-/-}$ mice developed myocardial hypertrophy without excessive fibrosis while *TIMP3*$^{-/-}$ mice showed elevated fibrosis with no hypertrophic response.[29] Our observation of increased collagen deposition without a proportional increase in myocyte size in the *OPN*$^{-/-}$ animals subjected to TAC highlights a potential disconnect between myocardial fibrosis and myocyte hypertrophy in this model.

Further studies are required to trace the OPN aptamer in different cell types, delineate the effect of the aptamer on extracellular versus intracellular OPN, and to compare the effects of OPN conditional genetic knock down versus pharmacological inhibition by OPN aptamer or

antibodies. Such studies may also elucidate the possibly different effects of targeting intracellular versus extracellular OPN. While previous studies of the OPN aptamer in cancer showed that the OPN aptamer works at the extracellular level in tumor cells with a short half life of less than 1 day in the blood,[21,22] the uptake of the OPN aptamer by non-tumor cells was not investigated. Whether the OPN aptamer is internalized in cardiovascular cells and could be used to deliver conjugated oligonucleotides like some aptamers could,[16–20] and whether the OPN aptamer has a different half life in cells versus circulation are all worthy of further investigation. Limitations of our study include the restriction to male mice rather than mixed genders. Also while our study investigated the effects of the OPN aptamer at 1–3 months after induction of TAC, it did not look at longer time points. It may also be useful to compare the effects of homozygous versus heterozygous genetic deletion of OPN in mice subjected to TAC.

In conclusion, our findings support a novel RNA platform for tuning down OPN pathologic signalling in cardiac hypertrophy and heart failure. The OPN aptamer technique may be applicable to other cardiac pathologies where OPN is activated. This study anticipates future investigations on OPN aptamer conjugation with other oligonucleotides such as siRNAs[16–18] and miRNAs[19,20] for potential targeted delivery or enhanced potency.

Supplementary material

Supplementary *Tables SI–SIV* and *Figures SI–SV* are available at *Cardiovascular Research* online.

Acknowledgements

We deeply thank Drs. Eli Gilboa and Randal Brenneman for the many intellectual and technical discussions on aptamers.

Conflict of interest: L.S. holds a patent on the use of Osteopontin aptamer to deliver oligonucleotides to cardiac, smooth muscle, endothelial, and progenitor cells.

Funding

This work was supported by the following grants to LAS: National Institute of Health (K01 AG040468), State of Florida (3KN05), Miami Heart Research Institute, and the American Heart Association (AHA) Grant-in-Aid (14GRNT19960000). W.D. is a recipient of a Sublett AHA predoctoral fellowship (15PRE22450019).

References

1. Kehat I, Molkentin JD. Molecular pathways underlying cardiac remodeling during pathophysiological stimulation. *Circulation* 2010;**122**:2727–2735.
2. McKinsey TA, Kass DA. Small-molecule therapies for cardiac hypertrophy: moving beneath the cell surface. *Nat Rev Drug Discov* 2007;**6**:617–635.
3. Singh K, Balligand JL, Fischer TA, Smith TW, Kelly RA. Glucocorticoids increase osteopontin expression in cardiac myocytes and microvascular endothelial cells. Role in regulation of inducible nitric oxide synthase. *J Biol Chem* 1995;**270**:28471–28478.
4. Graf K, Do YS, Ashizawa N, Meehan WP, Giachelli CM, Marboe CC, Fleck E, Hsueh WA. Myocardial osteopontin expression is associated with left ventricular hypertrophy. *Circulation* 1997;**96**:3063–3071.
5. Lorenzen JM, Schauerte C, Hubner A, Kolling M, Martino F, Scherf K, Batkai S, Zimmer K, Foinquinos A, Kaucsar T, Fiedler J, Kumarswamy R, Bang C, Hartmann D, Gupta SK, Kielstein J, Jungmann A, Katus HA, Weidemann F, Muller OJ, Haller H, Thum T. Osteopontin is indispensible for AP1-mediated angiotensin II-related miR-21 transcription during cardiac fibrosis. *Eur Heart J* 2015;**36**:2184–2196.
6. Ashizawa N, Graf K, Do YS, Nunohiro T, Giachelli CM, Meehan WP, Tuan TL, Hsueh WA. Osteopontin is produced by rat cardiac fibroblasts and mediates A(II)-induced DNA synthesis and collagen gel contraction. *J Clin Invest* 1996;**98**:2218–2227.
7. Renault MA, Robbesyn F, Reant P, Douin V, Daret D, Allieres C, Belloc I, Couffinhal T, Arnal JF, Klingel K, Desgranges C, Dos Santos P, Charpentier F, Gadeau AP. Osteopontin expression in cardiomyocytes induces dilated cardiomyopathy. *Circ Heart Fail* 2010;**3**:431–439.
8. Trueblood NA, Xie Z, Communal C, Sam F, Ngoy S, Liaw L, Jenkins AW, Wang J, Sawyer DB, Bing OH, Apstein CS, Colucci WS, Singh K. Exaggerated left ventricular dilation and reduced collagen deposition after myocardial infarction in mice lacking osteopontin. *Circ Res* 2001;**88**:1080–1087.
9. Collins AR, Schnee J, Wang W, Kim S, Fishbein MC, Bruemmer D, Law RE, Nicholas S, Ross RS, Hsueh WA. Osteopontin modulates angiotensin II-induced fibrosis in the intact murine heart. *J Am Coll Cardiol* 2004;**43**:1698–1705.
10. Lorenzen JM, Schauerte C, Hubner A, Kolling M, Martino F, Scherf K, Batkai S, Zimmer K, Foinquinos A, Kaucsar T, Fiedler J, Kumarswamy R, Bang C, Hartmann D, Gupta SK, Kielstein J, Jungmann A, Katus HA, Weidemann F, Muller OJ, Haller H, Thum T. Osteopontin is indispensible for AP1-mediated angiotensin II-related miR-21 transcription during cardiac fibrosis. *Eur Heart J* 2015;**36**:2184–2196.
11. Que-Gewirth NS, Sullenger BA. Gene therapy progress and prospects: RNA aptamers. *Gene Ther* 2007;**14**:283–291.
12. Ireson CR, Kelland LR. Discovery and development of anticancer aptamers. *Mol Cancer Ther* 2006;**5**:2957–2962.
13. Keefe AD, Pai S, Ellington A. Aptamers as therapeutics. *Nat Rev Drug Discov* 2010;**9**:537–550.
14. Banerjee J, Nilsen-Hamilton M. Aptamers: multifunctional molecules for biomedical research. *J Mol Med (Berl)* 2013;**91**:1333–1342.
15. Thiel KW, Giangrande PH. Therapeutic applications of DNA and RNA aptamers. *Oligonucleotides* 2009;**19**:209–222.
16. Berezhnoy A, Castro I, Levay A, Malek TR, Gilboa E. Aptamer-targeted inhibition of mTOR in t cells enhances antitumor immunity. *J Clin Invest* 2013;**124**:188–197.
17. Berezhnoy A, Brenneman R, Bajgelman M, Seales D, Gilboa E. Thermal stability of siRNA modulates aptamer- conjugated siRNA inhibition. *Mol Ther Nucleic Acids* 2012;**1**:e51.
18. Pastor F, Kolonias D, Giangrande PH, Gilboa E. Induction of tumour immunity by targeted inhibition of nonsense-mediated mRNA decay. *Nature* 2010;**465**:227–230.
19. Liu N, Zhou C, Zhao J, Chen Y. Reversal of paclitaxel resistance in epithelial ovarian carcinoma cells by a muc1 aptamer-let-7i chimera. *Cancer Invest* 2012;**30**:577–582.
20. Dai F, Zhang Y, Zhu X, Shan N, Chen Y. Anticancer role of MUC1 aptamer-miR-29b chimera in epithelial ovarian carcinoma cells through regulation of PTEN methylation. *Target Oncol* 2012;**7**:217–225.
21. Mi Z, Guo H, Russell MB, Liu Y, Sullenger BA, Kuo PC. RNA aptamer blockade of osteopontin inhibits growth and metastasis of MDA-MB231 breast cancer cells. *Mol Ther* 2009;**17**:153–161.
22. Talbot LJ, Mi Z, Bhattacharya SD, Kim V, Guo H, Kuo PC. Pharmacokinetic characterization of an RNA aptamer against osteopontin and demonstration of in vivo efficacy in reversing growth of human breast cancer cells. *Surgery* 2011;**150**:224–230.
23. Liaw L, Birk DE, Ballas CB, Whitsitt JS, Davidson JM, Hogan BL. Altered wound healing in mice lacking a functional osteopontin gene (spp1). *J Clin Invest* 1998;**101**:1468–1478.
24. Xie Z, Singh M, Singh K. Osteopontin modulates myocardial hypertrophy in response to chronic pressure overload in mice. *Hypertension* 2004;**44**:826–831.
25. Zhao M, Chow A, Powers J, Fajardo G, Bernstein D. Microarray analysis of gene expression after transverse aortic constriction in mice. *Physiol Genomics* 2004;**19**:93–105.
26. Emde B, Heinen A, Godecke A, Bottermann K. Wheat germ agglutinin staining as a suitable method for detection and quantification of fibrosis in cardiac tissue after myocardial infarction. *Eur J Histochem* 2014;**58**:2448.
27. Ashkar S, Weber GF, Panoutsakopoulou V, Sanchirico ME, Jansson M, Zawaideh S, Rittling SR, Denhardt DT, Glimcher MJ, Cantor H. ETA-1 (osteopontin): an early component of type-1 (cell-mediated) immunity. *Science* 2000;**287**:860–864.
28. Zhao H, Wang W, Zhang J, Liang T, Fan GP, Wang ZW, Zhang PD, Wang X. Inhibition of osteopontin reduce the cardiac myofibrosis in dilated cardiomyopathy via focal adhesion kinase mediated signaling pathway. *Am J Transl Res.* 2016;**8**:3645–3655.
29. Fan D, Takawale A, Basu R, Patel V, Lee J, Kandalam V, Wang X, Oudit GY, Kassiri Z. Differential role of TIMP2 and TIMP3 in cardiac hypertrophy, fibrosis, and diastolic dysfunction. *Cardiovasc Res* 2014;**103**:268–280.